



## How Coarsening the 3D Reconstruction of a Porous Material Influences Diffusivity and Conductivity Values

T. Hutzenlaub,<sup>a,z</sup> J. Becker,<sup>b</sup> R. Zengerle,<sup>a</sup> and S. Thiele<sup>a,\*</sup>

<sup>a</sup>Laboratory for MEMS Applications, IMTEK-Department of Microsystems Engineering, University of Freiburg, 79110 Freiburg, Germany

<sup>b</sup>Fraunhofer Institute for Industrial Mathematics (ITWM), 67663 Kaiserslautern, Germany

Coarsening the resolution of a 3D reconstruction is a common approach to make simulations feasible with regard to computational resources. We coarsen the reconstruction of a PEMFC cathode catalyst layer and investigate how this influences parameters such as diffusivity and conductivity. This is also an indication of how trustworthy these parameters are in the first place, because imaging itself is a coarsened representation of the real morphology. While diffusivity remains approximately constant due to the opposing behavior of bulk and Knudsen diffusivity, conductivity is strongly affected. The method introduced here is transferable to evaluate 3D reconstructions of other porous materials.

© 2012 The Electrochemical Society. [DOI: 10.1149/2.006302eel] All rights reserved.

Manuscript submitted October 2, 2012; revised manuscript received November 12, 2012. Published November 29, 2012.

Characterization by means of visual investigation is a common approach employed in polymer electrolyte membrane fuel cell (PEMFC) research. Depending on the point of interest, methods that differ in optical magnification and resolution are applied. This can vary from no magnification at all, such as transparent flow fields for viewing fluid streams in-situ,<sup>1</sup> to transmission electron microscopy (TEM) tomography<sup>2</sup> with resolutions below 1 nm, which allow visualization of platinum particles in the catalyst layer.<sup>3</sup>

In recent years, focused ion beam / scanning electron microscopy tomography (FIB/SEM)<sup>4</sup> has been utilized to study the microstructure of solid oxide fuel cells. Electrode material was removed layer by layer. Images of each layer were combined to achieve a three-dimensional reconstruction of the investigated electrodes.<sup>5-9</sup> This method was also subsequently applied to PEMFC catalyst layers<sup>10,11</sup> and allowed detailed differentiation of pore and bulk material. This in turn makes parameters accessible which cannot easily be determined experimentally for these materials, such as pore size distribution or effective diffusivity. These parameters can then be used in macrohomogeneous simulations.

However, depending on the method of calculation, there are also limits on how much data can be processed simultaneously to generate these parameters. In the case of the PEMFC catalyst layer reconstructed in,<sup>10</sup> the total reconstructed volume consists of almost one hundred and thirty million voxels. Especially simulation methods that rely on meshing are limited by today's computational possibilities and thus vastly overloaded by such a large number of calculation entities.<sup>12</sup> Additionally, it is often necessary to repeat simulations for extended parameter studies, which further reduces available time per simulation run.

The obvious solution is to reduce the number of voxels by resampling the images to a lower resolution, which we define as "coarsening". Nevertheless, this step also comes at the cost of further simplifying the reconstruction of the actual microstructure, potentially distorting results of the subsequently calculated parameters.

To analyze the effect of coarsening on a selection of typical parameters, we segment a stack of images of a PEMFC cathode catalyst layer (CCL) and resample the images step-by-step to a lower resolution. We calculate and compare porosity, specific surface area, average pore and grain diameter, diffusivity and conductivity for the different resolutions. This allows the original trustworthiness of the parameters to be assessed, because all imaging, even without a subsequent resampling step, is a simplified representation of the real microstructure. Though the approach described here was performed on a PEMFC CCL it is important to note that it is generic and easily transferable to other porous material systems.

### Experimental 3D Image Acquisition

The starting point for image acquisition by FIB/SEM was the cathode of a Gore PRIMEA A510.1 M710.18 C510.4 PEMFC membrane electrode assembly (MEA), which is commercially available. A cavity was cut into a sample of this material by FIB milling (Fig. 1a). Subsequently, the SEM was focused onto one of the side walls of this cavity and recorded images between FIB ablation steps that remove thin layers of material. The reconstruction procedure, including alignment, was performed analogously to Thiele et al.<sup>11</sup>

The result was a stack of 120 images with a resolution of 2.5 nm × 2.5 nm (x and y directions, the y direction describes the through-plane direction from the membrane to the gas diffusion layer) with an average spacing of 13.6 nm between images (z direction). As most calculation methods applied in this work demand cubic voxels, the images were resampled to 3.4 nm × 3.4 nm by linear interpolation and the z-direction scaled by 4, resulting in cubic voxels with an edge length of 3.4 nm. The stack was cropped to 1.632 μm × 1.632 μm × 1.632 μm and 480 × 480 × 480 voxels to remove unwanted edge effects and segmented with a semi-automatic approach that differentiates between pores and the solid phase.<sup>11,12</sup>

Small non-connected regions were eliminated from both phases by applying the bwareaopen function in Matlab<sup>13</sup> with a threshold of 10 pixels. Matlab was also employed to compare the effect of the definition of connectivity. The difference in connected porosity between 6-connected and 26-connected neighborhoods was determined to be less than 0.1%. The 6-connected definition was chosen for all further calculations.

All calculations in this work were performed on a Linux cluster with two AMD Opteron 12-core 2.1 GHz processors and 59 GB RAM.

### Resampling Mechanism

The binary 3D representation is resampled by "majority wins" interpolation where the geometrical model is divided into cubic sub-volumes with the size of the target voxel in a first step. Then the color that occurs more often in each sub-volume defines the color of the new voxel. At an equal count, the color of the new voxel is defined as the one which reaches 50% first according to the input sequence of the software used. Resampling factors of 0.5, 0.25, 0.125, 0.0625 and 0.03125 were investigated (Fig. 1b-1g), creating five additional 3D representations of the CCL with varying resolution and number of voxels. A resampling factor of 0.5 yields a cube consisting of 240 × 240 × 240 voxels with an edge length of 6.8 nm. At a resampling factor of 0.03125, the cube consists of 15 × 15 × 15 voxels with an edge length of 108.8 nm. The resampling function of the software ScanIP<sup>14</sup> is utilized to perform the coarsening.

\*Electrochemical Society Student Member.

<sup>z</sup>E-mail: tobias.hutzenlaub@imtek.de

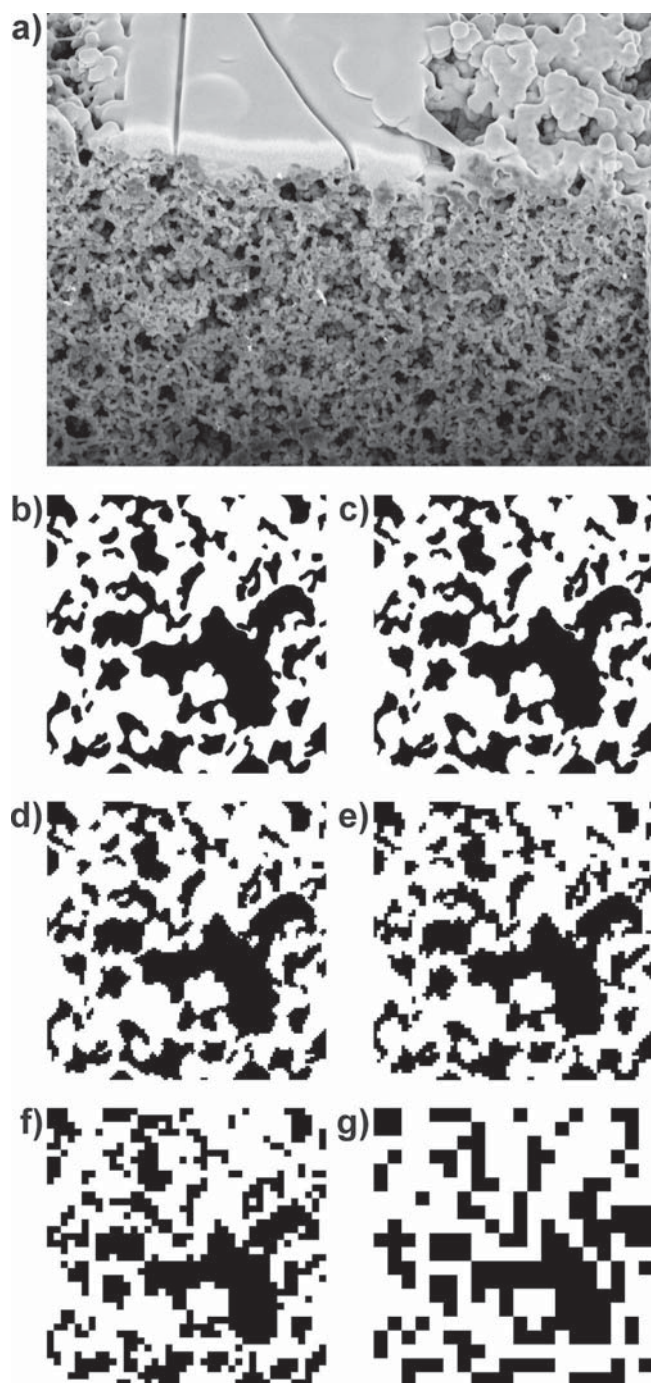


**Figure 1.** a) Cutting plane and sample surface recorded between two ablation steps at a camera angle of  $36^\circ$  with respect to the sample surface. b) Example of an image of the reconstructed stack with a resolution of  $480 \times 480$  pixels with a pixel edge length of 3.4 nm. c) – g) The image of Fig. 1b coarsened by employing the “majority wins” algorithm with a resampling factor of: c) 0.5 d) 0.25 e) 0.125 f) 0.0625 g) 0.03125.

### Methods and Results

**Porosity.**— The porosity is calculated by determining the number of voxels representing pore space and dividing this value by the total number of voxels in the 3D representation. The software GeoDict<sup>15</sup> is used as the calculation tool. The porosity remains constant at approximately 58% for all coarsening steps (Fig. 2a).

**Specific surface area.**— The surface area is determined by employing a method introduced by Ohser et al.<sup>16</sup> with GeoDict.<sup>15</sup> The

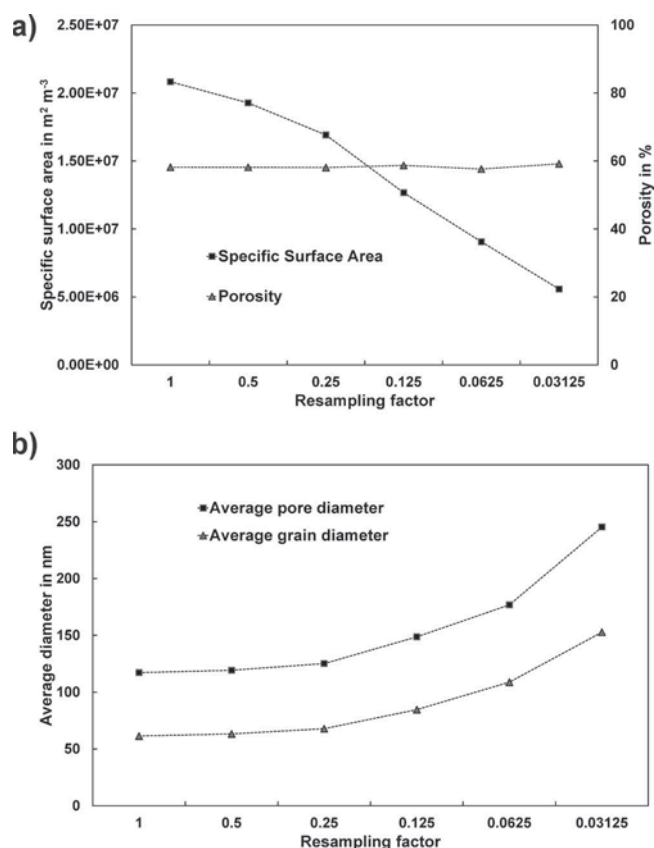


**Figure 2.** a) Specific surface area and porosity versus resampling factor. While the porosity stays approximately constant, the specific surface area is greatly reduced by the coarsening. b) Stronger coarsening increases both the average pore and grain diameter as the geometrical model loses its ability to resolve smaller pores.

method originates from statistical image analysis, where the determination of the four Minkowski measures (volume, surface area, integral of mean curvature, integral of total curvature) from voxelized images is an essential task. To determine the surface area, the Crofton formula is used, which relates the 3D surface area to an integral over 2D boundary lengths of planar cross sections. Then these lengths are related to an integral over 1D rays. Based on this formula an analysis of the intersection points of rays in all spatial directions of the structure allows the determination of the surface area. The specific surface area is derived by dividing the result of the surface area calculation by the volume of the 3D representation. As expected, the surface area is greatly reduced by coarsening with every resampling step. For a resampling factor of 0.03125, the specific surface area is reduced by 78% compared to the original representation (Fig. 2a).

**Average pore diameter and average grain diameter.**— The pore size distribution is calculated by using a method first described by Delerue et al.<sup>17</sup> implemented in GeoDict.<sup>15</sup> The grain size distribution is computed analogously by applying the same algorithm to the solid phase. From these distributions, an average pore diameter and an average grain diameter is derived for each coarsening step by calculating a weighted average over all intervals of the respective distribution (Fig. 2b). Both average pore diameter and average grain diameter are increased due to coarsening as the respective geometrical representations lose their ability to depict small pores and grains due to larger voxel sizes. This is especially the case for smaller resampling factors, while the diameters are increased only slightly by resampling factors of 0.5 and 0.25. This suggests that the original 3D image is a good representation of the real morphology with regard to both pore and grain diameter. At a resampling factor of 0.03125, the average grain

diameter is 2.5 times and the average pore diameter is 2.1 times higher than the values determined from the original 3D image.

**Diffusivity.**— The diffusion mechanism applicable to a porous medium can be determined by calculating the Knudsen number  $Kn$ :

$$Kn = \frac{\lambda}{l} \quad [1]$$

$\lambda$  is called the mean free path and describes the distance that a molecule travels between two successive intermolecular collisions. This is a specific value for a given gas under defined pressure and temperature conditions. It is noteworthy that this parameter is independent of the porous medium involved. By contrast,  $l$  is defined as a representative physical length scale of the porous medium investigated, e.g. an average pore diameter. Consequently,  $Kn \gg 1$  indicates that a gas molecule will predominantly collide with pore walls, whereas  $Kn \ll 1$  means that collisions between molecules are considerably more probable than collisions with the pore wall.

These two collision types are modeled by two different approaches. So-called Knudsen diffusion, where a molecule can only collide with walls, is modeled by a random walk approach.<sup>18,19</sup> The intermolecular collision case is called bulk diffusion and can be described by the well-known Fick's law.

Usually the more applicable mechanism for the physical length scale involved is identified and the other mechanism is neglected. However, at intermediate Knudsen numbers, as is the case in the reconstructed CCL, both mechanisms contribute significantly. Here a total effective diffusivity can be calculated by Bosanquet's formula:<sup>19,20</sup>

$$D_{\kappa} = ((D_{\kappa}^{Kn})^{-1} + (D_{\kappa}^{bulk})^{-1})^{-1} \quad \kappa = x, y, z \quad [2]$$

$D_{\kappa}^{bulk}$  is defined as the product of a dimensionless diffusivity  $D_{\kappa}^{bulk,*}$ , which depends only on the pore structure and the diffusion coefficient known from Fick's law for a gas in free space  $D^{bulk,0}$ :

$$D_{\kappa}^{bulk} = D_{\kappa}^{bulk,*} D^{bulk,0} \quad \kappa = x, y, z \quad [3]$$

Analogously  $D_{\kappa}^{Kn}$  can be divided into a dimensionless diffusivity  $D_{\kappa}^{Kn,*}$  and a diffusivity  $D^{Kn,0}$ . This allows to recalculate  $D_{\kappa}^{Kn}$  for an arbitrary gas by only changing the substance-specific value in  $D^{Kn,0}$ .

$$D_{\kappa}^{Kn} = D_{\kappa}^{Kn,*} D^{Kn,0} \quad \kappa = x, y, z \quad [4]$$

$D^{Kn,0}$  is calculated according to:

$$D^{Kn,0} = \frac{1}{3} l v_{mean} \quad [5]$$

$D^{bulk,0}$  is defined as the experimentally determined diffusion coefficient of oxygen in nitrogen.  $D^{bulk,0} = 2.086 \times 10^{-5} \text{ m}^2 \text{ s}^{-1}$ .<sup>18</sup>  $D_{\kappa}^{bulk,*}$  and  $D_{\kappa}^{Kn,*}$  are calculated with GeoDict<sup>15</sup> as described by Becker et al.<sup>19</sup> The physical length scale  $l$  is a result of the random walk simulation with GeoDict and is defined as the average distance between successive molecule-wall collisions. The mean thermal velocity is taken from the literature:  $v_{mean} = 444.1 \text{ ms}^{-1}$  (at 25°C and 191.3 kPa).<sup>19</sup> These values also allow the calculation of the Knudsen number which varies between 0.6 (resampling factor 0.03125) and 1.2 (original 3D representation).

These calculation steps were carried out for the original geometrical model and all coarsened models. The result is depicted in Fig. 3a. The effective diffusivity remains approximately constant for the first two coarsening steps and then rises slightly with lower resolution. This suggests that the original representation is well suited to calculate the diffusivity of the original sample.

This can be explained by the counteracting effects of coarsening on bulk and Knudsen diffusivity (Fig. 4a). On the one hand, bulk diffusivity is reduced in coarser representations. A possible explanation is that coarsened diagonals display increased tortuosity, which was demonstrated by comparing values of simple test cubes containing only one diagonal pore (Fig. 4b). On the other hand, Knudsen diffusivity is enhanced in coarser geometries. The reason for this can be understood directly by comparing Fig. 2b and Fig. 4a. For resampling factors of 0.5 and 0.25, the average pore diameter and the Knudsen

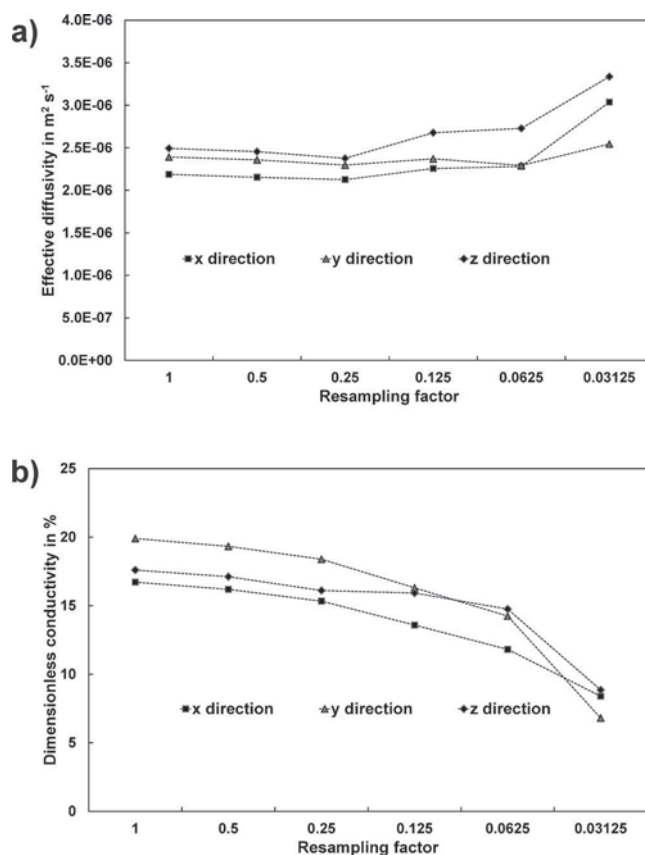


**Figure 3.** a) Effective diffusivity in all spatial directions for all resampling factors investigated in this work. The effective diffusivity is approximately constant for the first two coarsening steps and then rises slightly. b) Dimensionless conductivity in all spatial directions for all resampling factors investigated in this work. The dimensionless conductivity is reduced with coarsening of the resolution.

diffusivity do not change much, but for the smaller factors, both the average pore diameter and Knudsen diffusivity rise simultaneously. This is due to the fact that the Knudsen diffusivity in a cylindrical pore is proportional to the pore diameter, which is Knudsen's original result.<sup>21</sup> This counteracting effect is specific to this particular range of Knudsen numbers.

**Electric conductivity.**— The electric conductivity can be computed by a continuum approach applied to the solid phase of the 3D reconstruction. The pore space is assumed to be non-conducting. The effective conductivity  $\sigma_{\kappa}$  is defined as:

$$\sigma_{\kappa} = -\frac{I_{\kappa} L_{\kappa}}{\Delta \varphi_{\kappa} A_{\kappa}} \quad \kappa = x, y, z \quad [6]$$

with the electric potential difference  $\Delta \varphi$  and the length  $L$  from one face of the generated geometrical body to its opposite side, the corresponding cross-sectional area  $A$  and a resulting electric current  $I$ . The effective conductivity can be described as the product of a dimensionless conductivity  $\sigma_{\kappa}^*$ , which depends only on the structure of the solid phase, and a material-specific conductivity  $\sigma^0$ .

$$\sigma_{\kappa} = \sigma_{\kappa}^* \sigma^0 \quad \kappa = x, y, z \quad [7]$$

As  $\sigma^0$  is a constant value,  $\sigma_{\kappa}^*$  suffices to evaluate the effect of coarsening on conductivity. The dimensionless conductivity  $\sigma_{\kappa}^*$  in the x, y and z directions is calculated with GeoDict<sup>15</sup> for all geometrical images (Fig. 3b). The conductivity is strongly reduced by coarsening. This is very pronounced for smaller resampling factors, while factors 0.5 and 0.25 only slightly reduce the conductivity. This suggests that the original representation is a suitable starting point for conductivity

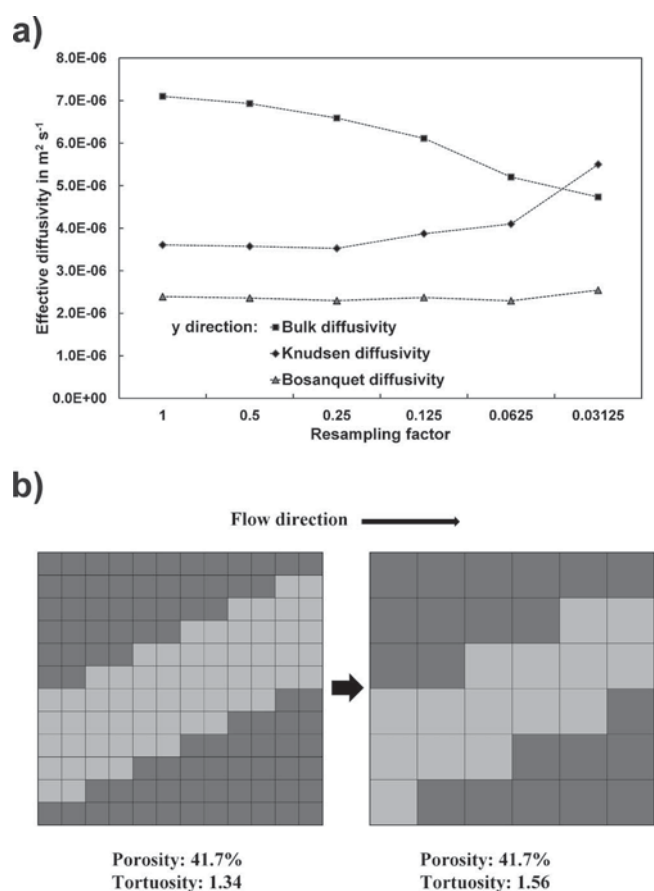


**Figure 4.** a) Bulk diffusivity, Knudsen diffusivity and total effective diffusivity in the y direction (the through-plane direction of the catalyst layer). While the Knudsen diffusivity yields higher values with lower resolution, the bulk diffusivity shows the reverse behavior. The result is an approximately constant total effective diffusivity. b) Cross-section of one diagonal pore in a test cube at two different resolutions (left:  $12 \times 12 \times 12$  voxels with an edge length of 1 nm; right:  $6 \times 6 \times 6$  voxels with an edge length of 2 nm). The tortuosity increases from 1.34 to 1.56 due to a reduced ability to depict diagonals even though the porosity remains at a constant value of 41.7%.

calculations. At a resampling factor of 0.03125, the conductivity in the y direction is 2.9 times lower than the value with the original representation. Analogously to the bulk diffusivity calculated in Section “Diffusivity”, a possible explanation is the increase in tortuosity along diagonal bulk material due to coarsening.

### Conclusions

We described a method to quantify the influence of resolution on common parameters calculated from geometrical models created by 3D reconstruction. This is important, not only because coarsening is often necessary to make a model computable in the first place, but also because imaging itself is a process where morphological information is simplified and averaged according to the available and employed resolution of the imaging device. In particular, specific surface area displays a strong dependence on resolution, thus suggesting that this parameter was not very trustworthy in the first place. The parameters, average grain and pore diameter and conductivity, only display this strong dependence at low resampling factors, indicating that the results for the original geometrical model are suitable for further use in macro-homogeneous simulations. Diffusivity at this length scale is very stable for all coarsening steps due to opposing trends for Knudsen and bulk diffusivity.

Subject of future work is to further evaluate 3D reconstruction methods by comparing results to experimentally generated data, where available. To support projects in this field, we will provide both the original and the resampled geometrical models in the form of image stacks upon request.

### Acknowledgments

This work is part of the project PEM-Ca-D (Grant No. 03SF0360D) and is funded by the German Federal Ministry of Education and Research (BMBF).

### List of Symbols

$A_k$	cross-sectional area of 3D reconstruction ( $\text{m}^2$ )
$D_k$	effective Bosanquet diffusivity ( $\text{m}^2 \text{s}^{-1}$ )
$D_k^{bulk}$	effective bulk diffusivity ( $\text{m}^2 \text{s}^{-1}$ )
$D_k^{Kn}$	effective Knudsen diffusivity ( $\text{m}^2 \text{s}^{-1}$ )
$D_k^{bulk,0}$	free, substance-specific bulk diffusivity ( $\text{m}^2 \text{s}^{-1}$ )
$D_k^{Kn,0}$	free, substance-specific Knudsen diffusivity ( $\text{m}^2 \text{s}^{-1}$ )
$D_k^{bulk,*}$	dimensionless bulk diffusion
$D_k^{Kn,*}$	dimensionless Knudsen diffusion
$I_k$	electric current (A)
$Kn$	Knudsen number (dimensionless)
$L_k$	length of 3D reconstruction (m)
$l$	physical length scale of the porous medium involved (m)
$v_{mean}$	thermal velocity ( $\text{m s}^{-1}$ )
$\kappa$	subscript defining spatial direction
$\lambda$	mean free path (m)
$\sigma_k$	effective conductivity ( $\text{S m}^{-1}$ )
$\sigma_k^0$	material-specific conductivity ( $\text{S m}^{-1}$ )
$\sigma_k^*$	dimensionless conductivity
$\varphi$	electric potential (V)

### References

- P. Argyropoulos, K. Scott, and W. M. Taama, *Journal of Applied Electrochemistry*, **29**, 661 (1999).
- D. B. Williams and C. B. Carter, *Transmission Electron Microscopy*, Springer (1996).
- H. Schulenburg, B. Schwanitz, N. Linse, G. G. Scherer, A. Wokaun, J. Krbanjevic, R. Grothausmann, and I. Manke, *The Journal of Physical Chemistry C*, **115**, 14236 (2011).
- L. Holzer, F. Indutnyi, P. H. Gasser, B. Munch, and M. Wegmann, *Journal of Microscopy*, **216**, 84 (2004).
- J. R. Wilson, W. Kobsiriphat, R. Menzona, H. Y. Chen, J. M. Hiller, D. J. Miller, K. Thornton, P. W. Voorhees, S. B. Adler, and S. A. Barnett, *Natural Materials*, **5**, 541 (2006).
- J. Joos, T. Carraro, A. Weber, and E. Ivers-Tiffée, *Journal of Power Sources*, **196**, 7302 (2011).
- D. Gostovic, J. R. Smith, D. P. Kundinger, K. S. Jones, and E. D. Wachsman, *Electrochemical and Solid-State Letters*, **10**, B214 (2007).
- J. R. Wilson, A. T. Duong, M. Gameiro, H. Y. Chen, K. Thornton, D. R. Mumm, and S. A. Barnett, *Electrochemistry Communications*, **11**, 1052 (2009).
- J. R. Wilson, J. S. Cronin, A. T. Duong, S. Rukes, H. Y. Chen, K. Thornton, D. R. Mumm, and S. Barnett, *Journal of Power Sources*, **195**, 1829 (2010).
- C. Ziegler, S. Thiele, and R. Zengerle, *Journal of Power Sources*, **196**, 2094 (2011).
- S. Thiele, R. Zengerle, and C. Ziegler, *Nano Research*, **4**, 849 (2011).
- T. Hutzenlaub, S. Thiele, R. Zengerle, and C. Ziegler, *Electrochemical and Solid-State Letters*, **15**, A33 (2012).
- www.mathworks.com, 2012.
- www.simpleware.com, 2012.
- www.geodict.com, 2012.
- J. Ohser and F. Muecklich, *Statistical Analysis*, Wiley & Sons (2000).
- J. F. Delerue, E. Perrier, Z. Y. Yu, and B. Velde, *Physics and Chemistry of the Earth Part A - Solid Earth and Geodesy*, **24**, 639 (1999).
- H. Babovsky, *Journal of Statistical Physics*, **44**, 865 (1986).
- J. Becker, C. Wieser, S. Fell, and K. Steiner, *International Journal of Heat and Mass Transfer*, **54**, 1360 (2011).
- W. G. Pollard and R. D. Present, *Physical Review*, **73**, 762 (1948).
- M. Knudsen, *Annalen der Physik*, **333**, 75 (1909).